Thermodynamic and kinetic properties of the Li-graphite system from first-principles calculations

Citation: Persson, Kristin et al. "Thermodynamic and kinetic properties of the Li-graphite system from first-principles calculations." Physical Review B 82.12 (2010): n. pag. c2010 The American Physical Society

As Published: http://dx.doi.org/10.1103/PhysRevB.82.125416

Publisher: American Physical Society

Persistent URL: http://hdl.handle.net/1721.1/60959

Version: Final published version: final published article, as it appeared in a journal, conference proceedings, or other formally published context

Thermodynamic and kinetic properties of the Li-graphite system from first-principles calculations

Kristin Persson,[1] Yoyo Hinuma,[2] Ying Shirley Meng,[2] Anton Van der Ven,[3] and Gerbrand Ceder[4]
[1]*Lawrence Berkeley National Laboratory, 1 Cyclotron Rd., Berkeley, California 94720, USA*
[2]*University of California–San Diego, Atkinson Hall 2703, La Jolla, California 92093, USA*
[3]*University of Michigan, Ann Arbor, Michigan 48109, USA*
[4]*Massachusetts Institute of Technology, 77 Massachusetts Avenue, Cambridge, Massachusetts 02139, USA*
(Received 19 January 2010; revised manuscript received 23 April 2010; published 9 September 2010)

We present an *ab initio* study of the thermodynamics and kinetics of Li_xC_6, relevant for anode Li intercalation in rechargeable Li batteries. In graphite, the interlayer interactions are dominated by Van der Waals forces, which are not captured with standard density-functional theory (DFT). By calculating the voltage profile for Li intercalation into graphite and comparing it to experimental results, we find that only by correcting for vdW interactions between the graphene planes is it possible to reproduce the experimentally observed sequence of phases, as a function of Li content. At higher Li content the interlayer binding forces are increasingly due to Li-C interactions, which are well characterized by DFT. Using the calculated energies, corrected for the vdW interactions, we derive an *ab initio* lattice model, based on the cluster-expansion formalism, that accounts for interactions among Li ions in Li_xC_6 having a stage I and stage II structure. We find that the resulting cluster expansions are dominated by Li-Li repulsive interactions. The phase diagram, obtained from Monte Carlo simulations, agrees well with experiments except at low Li concentrations as we exclude stage III and stage IV compounds. Furthermore, we calculate Li migration barriers for stage I and stage II compounds and identify limiting factors for Li mobility in the in-plane dilute as well as in the high Li concentration range. The Li diffusivity, obtained through kinetic Monte Carlo simulations, slowly decreases as a function of Li content, consistent with increasing Li-Li repulsions. However, overall we find very fast Li diffusion in bulk graphite, which may have important implications for Li battery anode optimizations.

DOI: 10.1103/PhysRevB.82.125416 PACS number(s): 66.30.−h, 65.40.G−, 71.15.Nc

I. INTRODUCTION

Graphitic carbon is the most commonly used anode in rechargeable Li batteries.[1] Also, graphitic environments are present, to some extent, in almost all carbon classes—microporous hard, soft carbons with turbostratic disorder, hydrogen containing, and graphitic[1,2]—which makes the graphite intercalation mechanism and its inherent limitations relevant to all of them. The Li-graphite temperature—composition phase diagram has been extensively explored, using both electrochemical and chemical lithiation synthesis techniques (see Refs. 3–8 and references therein) as well as modeling approaches.[8,9] As a function of increasing Li concentration, the Li-graphite intercalation occurs in stages, where stage *n* contains *n* empty layers between each Li-filled layer[2,6,10–12] (see Fig. 1 for illustrations of the Li-C stacking in stages I and II). This is different from, for example, intercalated transition-metal dichalcogenides which fill every layer with a continuously variable Li content.[13] In graphite, individual graphene sheets are composed of strong covalently bonded carbon atoms forming a honeycomb network. However, the only binding forces between the graphene sheets are due to weak Van der Waals (vdW) interactions. As Li intercalates, the hybridization between the Li valence electrons and graphite interlayer states—although weak in character (see Ref. 12 and references therein)—perturb and screen the C-C vdW bonds, which is evidenced in the change from *AB* hexagonal stacking (graphite) to *AA* stacking.[6,13,14] Thus, as a function of increasing Li content, the nature and strength of the interlayer bonding in the Li-graphite systems changes, as there is an increase in the number of Li-C bonds and a corresponding decrease in C-C vdW interactions. Given the importance of carbon as a Li-ion anode material, it is vital to fully understand the competition between these interactions, which is manifested in the Li-graphite phase diagram and the voltage profile. Despite the implications for Li battery rate performance and a multitude of experiments (see Refs. 15–17 and references therein), there are uncertainties regarding the kinetics of Li intercalation in carbon, and reported diffusivity measurements span a very wide range of 10^{-6}–10^{-14} cm^2/s.[15–17] Understanding where this discrepancy comes from and identifying inherent Li diffusivity limitations in graphite is imperative in order to fully optimize carbon materials for Li battery rate performance. First-principles calculations have previously elucidated the inherent kinetic capabilities in other systems, such as $LiFePO_4$,[18] and thereby enabled a targeted optimization of the material.[19] Verbrugge *et al.*[20] treated the Li diffusivity in graphite within the one-dimensional continuum transport framework and Toyoura *et al.*[21,22] recently calculated the Li diffusivity in ordered LiC_6 assuming a single vacancy or

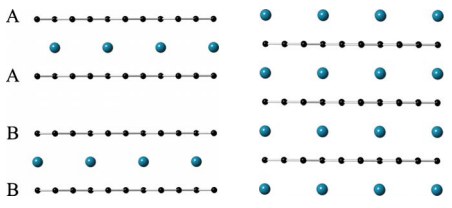

FIG. 1. (Color online) (a) 001 Li-C stacking in stage II (left) and (b) stage I (right). Note that in stage II, because of the AABB alternating graphite plane sequence, the Li atoms are not quite aligned in the 001-direction.

interstitial diffusion mechanism. However, the chemical diffusion coefficient of lithium as a function of concentration has not been calculated from first principles. Furthermore, there have been numerous *ab initio* studies performed on the electronic structure of LiC_6 and on the stacking of Li-intercalated graphite[14,22–27] as well as a recent investigation[9] of the Li-graphite stage II+stage I phase equilibrium using defect state calculations and a cluster [nearest-neighbor (NN)] configurational entropy model but neglecting vdW interactions.

We believe that the technological importance of the Li-graphite system warrants a detailed investigation of the Li-graphite system to understand the interactions governing the intercalation and to quantify the inherent Li diffusivity in the system. This work aims to use first-principles calculations to (1) understand the interactions governing the phase sequence in the Li-graphite system as a function of Li content (2) reproduce the experimental voltage profile and phase diagrams (2) and (3) obtain a clear picture of Li diffusivity in bulk graphite. As standard DFT treatments of graphite neglect vdW forces,[28] we choose to focus our investigation on the higher Li content phases (stages I and II) where the number of empty layers is minimized. By incorporating a simple constant vdW binding energy for every empty graphite layer in stage II, it is possible to study the phase diagram from $x > 0.5$ in Li_xC_6, and thereby elucidate the competing forces in the Li-graphite system.

II. METHODOLOGY

A. Ground-state properties

We calculate all structural energies through the generalized gradient approximation (GGA) (Ref. 29) to DFT as implemented in the Vienna *ab initio* simulation package (VASP).[30] Due to the lack of binding force between graphene planes in GGA,[28] the interlayer distance for empty grapheme-graphene layers is fixed to the experimental value of 3.35 Å.[15] However, at moderate intralayer Li concentrations the Li-C interactions, which are well described within the DFT framework, dominate over the vdW forces. Thus, for Li-containing layers, the interlayer distance is well reproduced. It has been argued that the local density approximation (LDA) spuriously mimics a fraction of the vdW interaction (see Ref. 31 and references therein), which would improve the treatment in graphite and the low Li concentration part of the phase diagram. However, LDA also severely overestimates the Li-C binding,[24] which impacts both the relative phase stability between the staged compounds as well as the Li migration barriers. Because we are more interested in obtaining the correct order of magnitude for the binding energetics in the high Li concentration range, we have chosen to use the GGA. Furthermore, projected augmented wave pseudopotentials were used with an energy cutoff of 400 eV. Only stage I and stage II Li-graphite phases were explored. Apart from the fixed interlayer distance for empty graphene-graphene layers, all internal coordinates and unit cell lattice parameters were fully relaxed. The Brillouin zones were sampled with a gamma-centered mesh so that the energy[32,33] convergence with respect to the *k*-point sampling was better than 5 meV/6C. For example, in *AB* stacked graphite this convergence requires a *k* mesh of $19\times19\times5$ and $11\times11\times11$ for the minimal unit cell in LiC_6. The density of the mesh for all calculations is approximately one point per 0.003 $Å^{-3}$. We calculated the energies of 63 different Li-vacancy arrangements in stage I and stage II forms of Li_xC_6. For stage I, both the graphite and Li layers had an *AA* stacking sequence[27] while in stage II, non-Li containing graphite layers had an *AB* stacking sequence. Construction of the convex hull to the formation energies relative to C_6 and Li_xC_6 (see Fig. 2) yielded the zero-temperature ground states as a function of Li concentration, presented in Table I.

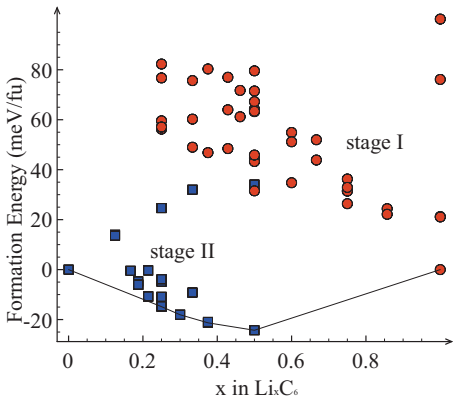

FIG. 2. (Color) First-principles calculated ground states from combined stage I (red circles) and stage II (blue squares) compounds. Stage II compound energies are shifted down by the vdW correction (20 meV/C) for every empty layer. The convex hull including both stage I and stage II compounds is indicated by the black line. It should be noted that the $x=0.25$ compound is very close to but not actually on the hull.

B. Cluster expansion of Li-vacancy interactions

We used the cluster-expansion method to model partially disordered states at finite temperatures. This methodology is well established for alloys,[34–39] and has previously been used to study Li/vacancy disorder in layered intercalation compounds such as Li_xCoO_2,[40,41] Li_xNiO_2,[42] $Li_xNi_{0.5}Mn_{0.5}O_2$,[43,44] Na_xCoO_2,[45] and Li_xTiS_2.[46] The Li sites are represented by a lattice model, with occupation variables, σ_i, assigned to each Li site i, which is +1 if occupied by Li and −1 when vacant. The essential idea is to expand the energy of the system in terms of polynomials of the occupation variables according to

$$E_\nu^{predict} = C + \sum_i V\sigma_i + \sum_{ij} V^{ij}\sigma_i\sigma_j + \cdots . \quad (1)$$

Here, $E_\nu^{predict}$ is the predicted energy for structure ν and C is a constant. The V^{ij} are effective cluster interactions (ECIs) corresponding to a cluster of sites with indices i and j. Separate cluster expansions were constructed for stage I structures (Li between every carbon layer) and stage II structures (Li in every second layer), respectively. While, in principle, the expansion of Eq. (1) has to be summed over all pairs, triplets, quadruplets, and larger clusters of sites, in practice relevant

TABLE I. Ground-states properties as obtained by first-principles calculations on stage I and stage II compounds. The formation energy of the compounds is calculated as $E_{form}(Li_xC_6)=E(Li_xC_6)-E_{graphite}(C_6)-xE_{Li\ metal}(Li)$. The c lattice parameters are given as averages between lithiated and empty planes, to facilitate comparison with experiments. The graphene planes consists of hexagons with sides $a/\sqrt{3}$, where $a_{calc}=2.497$ Å ($a_{exp}=2.46$ Å).

Compound class	x (in Li_xC_6)	Li ordering (a)	E_{form} (meV/6C)	c_{calc} (Å)	c_{exp} (Å)
Graphite	0		0	3.35[a]	3.35 (Ref. 15)
Stage II	0.3	$7/3\times\sqrt{3}$	−13.5	3.70	3.53 (Ref. 15)
Stage II	0.375	2×2	−16.0	3.70	3.53 (Ref. 15)
Stage II	0.5	$\sqrt{3}\times\sqrt{3}$	−18.2	3.70	3.53 (Ref. 15)
Stage I	1	$\sqrt{3}\times\sqrt{3}$	0	3.76	3.70 (Ref. 15)

[a]The graphite c lattice parameter was fixed to the experimental value, as the GGA does not contain any binding energy in the c direction.

cluster interactions can be selected on the basis of how well they minimize the weighted cross-validation (CV) score, which is a means of measuring how good the cluster expansion is at predicting the energy of structures not included in the fit.[47] Truncation amounts to neglecting any configurational details beyond a certain range on the energy and only including an average interaction. The cluster expansion is obtained through an iterative approach, whereby energies of newly predicted ground-state candidate structures and other relevant structures suggested by previous cluster expansions, are added into the training set of energies and structures used to fit the ECIs. Structures with different shape and size were calculated to search for ground states. Although automated schemes to find relevant structures to include in the cluster-expansion training set exist, such as in the MAPS code,[47] structures were picked "by hand." Structures similar to those with energies on or close to the convex hull were investigated in detail and were more heavily weighted in obtaining the CV score.

The final stage I cluster expansion was fitted to the energies of 44 different Li-vacancy configurations and the final stage II cluster expansion was fitted to the energies of 19 different Li-vacancy configurations. The maximum unit cell in stage I was 8 Li_xC_6 f.u. and 16 Li_xC_6 f.u. for stage II. Figure 3 illustrates the in-plane $\sqrt{3}\times\sqrt{3}$ Li ordering in fully lithiated stage I and stage II [Fig. 3(a)] and a 2×2 in-plane Li ordering [Fig. 3(b)].

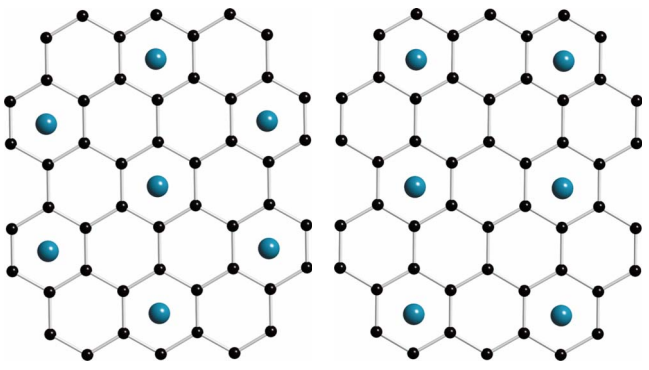

FIG. 3. (Color online) (a) In-plane Li ordering in fully lithiated stage I and stage II (left) and (b) 2×2 Li ordering (found in stage II′) (right) seen from above on the carbon honeycomb lattice.

C. Monte Carlo simulations

Grand canonical and canonical Monte Carlo simulations based on the METROPOLIS algorithm were applied to the cluster expansions to (1) obtain a set of ground states consistent with the first-principles data and (2) calculate the phase diagram. To explore in-plane orderings, for a given stage, Monte Carlo cells of dimensions $18\times18\times2$ (containing approximately 650 f.u.) were used. The Monte Carlo temperature scans at constant chemical potential were performed using 20 000 sampling passes with 5000 equilibrium passes at 10 K intervals. Constant temperature runs were calculated with at least 10 000 sampling passes and 2000 equilibrium passes. Some transition temperatures were obtained by looking at discontinuities in concentration or formation energies while others were obtained by free energy integration. Further details about the Monte Carlo technique and treatment of the data can be found in Ref. 45.

Kinetic Monte Carlo simulations were employed to calculate Li diffusion coefficients as a function of Li concentration in stage I and stage II compounds. The "chemical-diffusion" coefficient (intrinsic coefficient) D_C, which determines macroscopic diffusion as defined by Fick's law, can be factored according to

$$D_C = \Theta D_J, \tag{2}$$

where Θ is the thermodynamic factor, $\Theta=[\partial(\mu/k_BT)/\partial\ln x]$ and D_J is the jump diffusion coefficient

$$D_J = \lim_{t\to\infty}\left[\frac{1}{2dt}\left\langle\frac{1}{N}\left(\sum_{i=1}^{N}\vec{r}_i(t)\right)^2\right\rangle\right]. \tag{3}$$

In Eq. (3), $\vec{r}_i$ denotes the displacement of ith lithium ion after time t, N corresponds to the number of diffusing Li ions, and d is the dimension of the network that the diffusion occurs on ($d=2$ for graphite). The "jump-diffusion" coefficient (diffusion coefficient) is frequently approximated (as in this work) by the "tracer-diffusion" (random coefficient) coefficient

$$D^* = \lim_{t\to\infty}\left[\frac{1}{2dt}\left(\frac{1}{N}\sum_{i=1}^{N}\langle[\vec{r}_i(t)]^2\rangle\right)\right],$$

which neglects cross correlations between displacements of different particles. The trajectories $\vec{r}_i$ can be calculated in kinetic Monte Carlo simulations provided an accurate description of elementary hop events is available. We can approximate the frequency with which Li ions move to vacant neighboring sites with transition state theory according to

$$\Gamma = \upsilon^* \exp(-\Delta E_k/k_B T),$$

where ΔE_k is the difference between the energy at an activated state and the initial equilibrium state and υ^* is an effective vibrational frequency, here taken as 1×10^{13} s^{-1}, which is carefully calculated in Ref. 22 from first principles. The Li migration barriers in graphite are highly dependent on the local arrangement of Li ions. Therefore, when calculating the migration it is important that the hopping ions are far enough from their images within the DFT computational unit cell to ensure that the energy barriers truly model single ion hops. The DFT calculations of migration barriers were therefore performed in super cells where the hopping ions were at least 7 Å apart in-plane and at least one nonhopping Li layer or empty layer between every layer with hopping ions. The location and energy of the activated states were determined by the nudged elastic band method,[48] as implemented in VASP. The migration barriers were combined with the cluster expansion[49] for the Li-vacancy configurational energy in graphite and used to construct activation barriers in kinetic Monte Carlo simulations to calculate the Li diffusion coefficient, Eq. (2). The diffusion coefficients were obtained through kinetic Monte Carlo simulations using $12\times12\times12$ cells at a fixed temperature of 300 K using 1000 sampling passes with 500 equilibrium passes and 50 ensemble averages. The thermodynamic factor Θ in Eq. (2) was calculated with grand canonical Monte Carlo simulations as described in Refs. 46 and 49.

III. RESULTS AND DISCUSSION

A. Li-vacancy cluster expansion

Figures 4 and 5 show the clusters included in the CE for stage I and stage II. Only pair interactions were found to be necessary to reproduce the ground states of the Li-graphite system. For stage I both in-plane and next-plane interactions were included up to 5 Å. It was especially important to include the NN pair interaction, which is highly repulsive and dominates in both stage I and stage II compounds. Thus, this repulsive interaction sets the intercalation capacity limit for graphitic carbon materials to LiC_6. As a reference, the Li-Li NN in-plane distance in graphite is 2.5 Å, which should be compared with the shortest Li-Li distance in Li metal of 3.04 Å. From Fig. 4 we note that both in-plane and out-of-plane stage I interactions are repulsive and rapidly decaying. This choice of clusters for the stage I CE resulted in a weighted CV score of 22.4 meV/6C and an rms of 8.8 meV/6C. The Li ordering of the first-principles calculated ground states matches the ground states obtained in the CE.

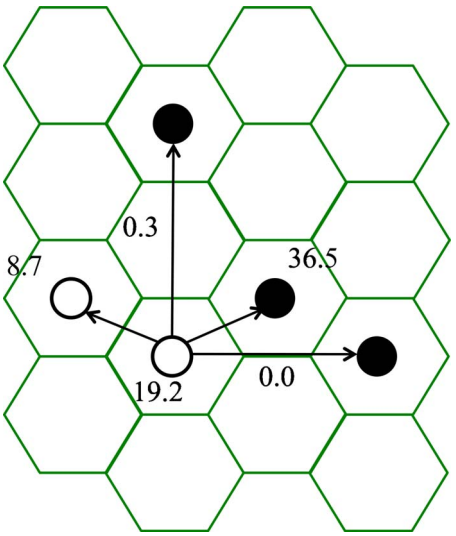

FIG. 4. (Color online) Pairwise ECI for the stage I CE illustrated on the honeycomb carbon lattice. Filled circles represent in-plane interactions while open circles represent next-plane interactions. The numbers denote the magnitude of the ECIs in meV.

For stage II only in-plane interactions were included (see Fig. 5) as the NN out-of-plane interaction connecting Li sites would have to extend over an empty layer (more than 7.4 Å). As can be deduced from the stage I CE, this interlayer ECI would be negligible. Figure 5 shows the clusters with their respective ECI for the stage II CE, which is completely dominated by the repulsive NN interaction. By this scheme, stage II exhibits a weighted CV score of 4.6 meV/6C and an rms of 2.5 meV/6C. As for stage I, the first-principles calculated stage II ground state Li orderings match those obtained with the CE.

From the CEs we conclude that, in both stage I and stage II the Li-Li interactions and resulting ordering are dominated by simple short-range repulsive electrostatic interactions.

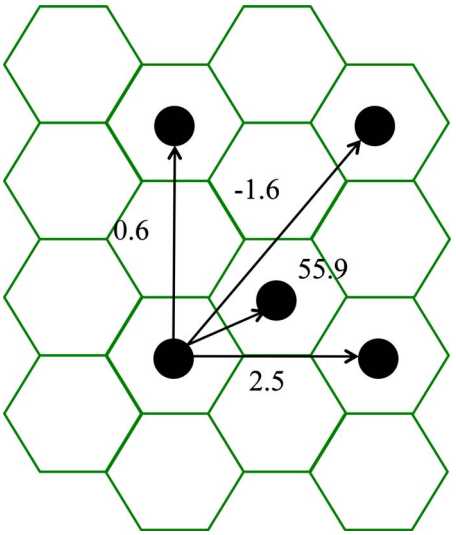

FIG. 5. (Color online) Pairwise Li-Li ECI for the stage II CE illustrated on the honeycomb carbon lattice. Filled circles represent in-plane interactions while open circles represent next-plane interactions. The numbers denote the magnitude of the ECIs in meV.

This is similar to findings in Ref. 9, where isolated Li-Li pair energies in graphite are calculated as a function of site and range. Early modeling based on analytical Thomas-Fermi equations[8] suggested that the Li-graphite stage ordering could result from attractive interactions between Li in different layers. We see no evidence of such interactions. Instead we find that the stage ordering in the Li-graphite system originates from a competition in interactions, as evidenced in Sec. III B. As Li intercalates, the interlayer C-C vdW forces decreases while Li-Li repulsion increases. This competition in interactions, as a function of Li content, governs the sequence of stable phases in the system. As discussed previously, the vdW term is not captured in standard DFT and will have to be accounted for in another way. We chose to model this competition by simply incorporating a constant vdW correction that promotes empty graphite layers. In practice, this scheme reduces to adding a constant attractive energy term to the total energy of every stage II compound which will not impact the separate CEs but will promote empty layers compared to dilute in-plane lithiation as well as affect the relative stability of stage II versus stage I phases. In Ref. 50 the binding energy in graphite is experimentally determined as 35^{+15}_{-10} meV/atom. Given that we are modeling Li-C systems and the Li is likely to perturb the vdW forces, we chose a correction term on the lower end of the measured energy binding strength (20 meV/C for every empty graphene-graphene layer), which still matches the correct order of magnitude for the graphite interlayer binding energy.

B. Li-graphite voltage profile

The average potential as a function of Li intercalation content in a material is calculated as

$$V(x) = -\frac{G(\mathrm{Li}_{x_1}\mathrm{C}_6) - G(\mathrm{Li}_{x_0}\mathrm{C}_6) - (x_1 - x_0)G(\mathrm{Li})}{x_1 - x_0},$$

where G is the Gibbs free energy of the compound. The Gibbs energy can be replaced with ground-state energies with little error.[51] Thus, the voltage profile reflects the sequence of stable phases in the system, as the phase transitions give rise to plateaus in the potential vs Li content.[3] Figure 6 shows the comparison between the experimental voltage profile[2] in $\mathrm{Li}_x\mathrm{C}_6$ and the one obtained using standard DFT energies as well as DFT energies corrected for vdW interactions. In the voltage profile obtained from the uncorrected DFT data we find that stage II is favorable at low Li concentrations, compared to stage I, due to the repulsive Li-Li interaction across one graphite plane, which is seen from the stage I CE (see Fig. 4). However, the stage II to stage I two-phase region starts at too low a Li composition, $x=0.23$ compared to an experimental value of $x=0.5$. Also, the voltage profile obtained from the uncorrected calculations is too steep at low Li content, promoting very dilute stage II compounds with different in-plane Li concentrations, a phenomenon which is not seen experimentally.[3] This can be easily understood when considering the lack of vdW interactions between the graphene planes. Experimentally, it has been deduced that in-plane Li screens the van der Waals interactions.[14,15] Thus, there is a competition between attractive van der Waals interactions which prefers to keep planes free of Li and the attractive Li-C interactions which promote Li intercalation and lastly, Li-Li repulsion which prefer to put Li ions as far apart as possible (and hence in all planes). The delicate balance between the three interactions result in a critical Li concentration for which there is enough thermodynamic driving force to open up and start populating an empty grapheme-graphene layer. By neglecting the vdW interactions in the Li-graphite system, (as given by standard DFT calculations), there is no incentive to keep graphene-graphene planes empty compared to filling them with dilute levels of Li.

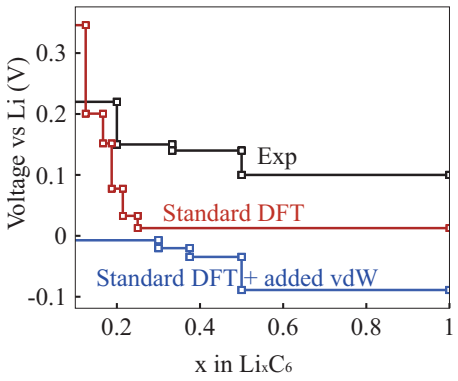

FIG. 6. (Color) Voltage profile for the Li-graphite system obtained by standard DFT data (red line), DFT data corrected for vdW interactions (blue line), compared to experiments (black curve) (Ref. 2).

Adding a simple constant vdW energy correction of 20 meV/C for every empty layer greatly improves the phase sequence with increasing Li concentration, i.e., the voltage profile (see Fig. 6), compared to experiments. The first lithiated phase to become thermodynamically favorable is now a dilute stage II compound ($x=0.3$) and the stage I+stage II two-phase region starts at $x=0.5$, in agreement with experiments. On the other hand, this simplified model, with a constant vdW energy promotion term, also leads to a slight overstabilization of the graphite phase and a resulting downward shift of the voltage profile by approximately 0.2 V. However, this could be simply corrected by modifying the external chemical potential of Li and it is more important that the relative stability of the phases, i.e., the shape of the voltage profile, is accurate.

C. Li-graphite phase diagram

Monte Carlo simulations were performed on stage I and stage II phases separately and the phase diagram was obtained by combining the free energies from both sets of simulations. Figure 7 shows the phase diagram obtained from the stage I and stage II CE including the vdW correction for the stage II phases. At high Li content we find that the phase diagram agrees very well with experiments,[3–7] which validates our simple CE and treatment of the vdW interactions. Starting with the fully lithiated compound at $x=1$, we find that the ordered LiC_6 stage I disorders at 780 K. This agrees very well with experimental observations[5] that

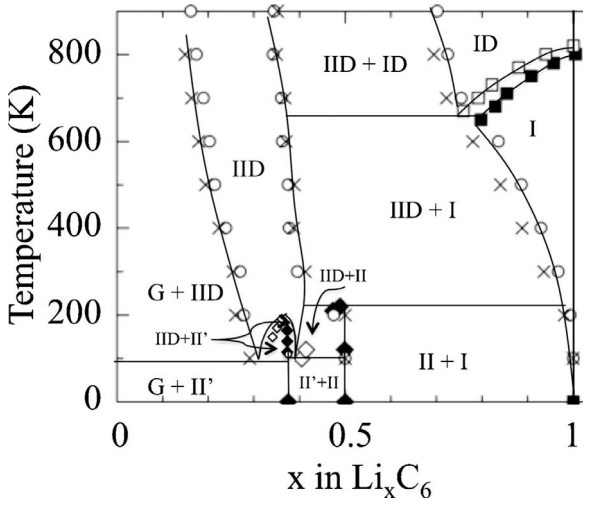

FIG. 7. First-principles phase diagram obtained from Monte Carlo simulations based on stage I and stage II separate CEs. The phase regions are denoted in the following way: G (graphite), II (stage II), IID (disordered stage II), I (stage I), ID (disordered stage I), and II′ (stage II with 2×2 Li ordering—see Fig. 3(b). Different symbols refer to cooling and heating runs, respectively.

stage I at $x=0.99$ disorders at 715 K. The stage II ordered configuration ($x=0.5$), disappears through a peritectoid reaction at 250 K, which is well reproduced compared to experiments (150 K).[7] Similarly, we find that the two-phase ordered stage I+II region for $0.5<x<1$ transitions to a disordered stage II+ordered stage I two-phase region at 250 K, to be compared with 150 K experimentally.[7] However, at higher temperatures ($T>500$ K) Woo *et al.*[5] observes a broader stability of disordered stage I ($0.5<x<0.99$) compared to our calculations ($0.8<x<1$) for $T>650$ K. At $x=0.375$ we find that the calculated stable phase at low temperature is a dilute stage II (II′) compound with 2×2 in-plane Li ordering [see Fig. 3(b)]. This phase disorders at 100 K. Similarly, experiments[2,6] find that stage II+stage III disorders through a eutectoid at ~270 K into a dilute stage II phase with short-range 2×2 in-plane Li ordering (here denoted II′).

Generally, for $x<0.5$, we cannot expect to obtain correct results as we are only allowing stage I and stage II phases in

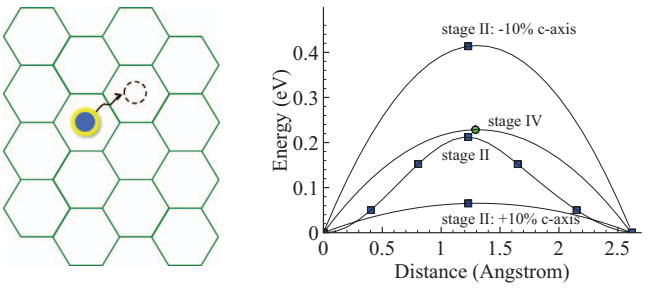

FIG. 8. (Color) [(a) and (b)] The picture to the left (a) schematically illustrates an in-plane Li hop from one site to an adjacent one and (b) shows the corresponding energy barriers for this path in dilute stage II and stage IV calculated from first principles for different c lattice parameters (equilibrium, 10% expanded and 10% contracted interlayer distance).

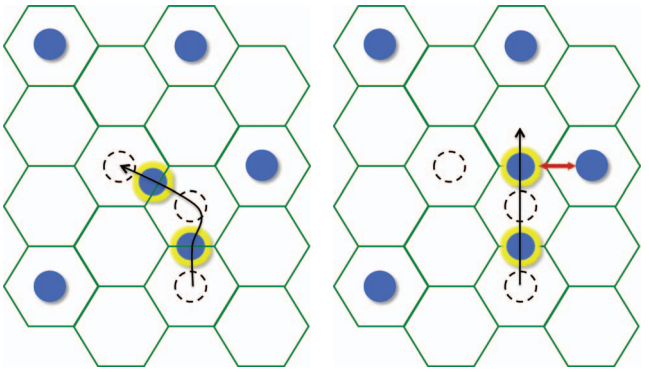

FIG. 9. (Color) [(a) and (b)] The pictures schematically illustrate how the Li moves in-plane from one site, through an adjacent nearest-neighbor site, to a vacancy—the left-hand "vacancy" hop in (a)—or a NN site—the right-hand NN hop in (b)—under high Li concentration conditions. The migrating Li are shown as highlighted blue circles and the trajectories are indicated by arrows and dashed circles. The NN hop is energetically extremely unfavorable, compared to the vacancy hop.

our simulations. However, it is worth noticing that some broad features manifest similarly in the calculated phase diagram as compared to the experimental results. Between $x=0-0.375$ we observe a graphite+stage II′ two-phase region which disorders at 100 K. This can be compared to the graphite+stage IV two-phase region seen in experiments,[3] which occurs between $0<x<0.15$ and disorders around 200 K.

D. Li diffusion in the Li-graphite system

Lithium motion in graphite is restricted to two-dimensional diffusion; hopping between layers through a perfect carbon honeycomb is energetically extremely unfavorable (approximately 10 eV).[52] Thus, we calculated the *intralayer* Li migration barriers in stage I and stage II compounds. We separate the compounds into two cases: very

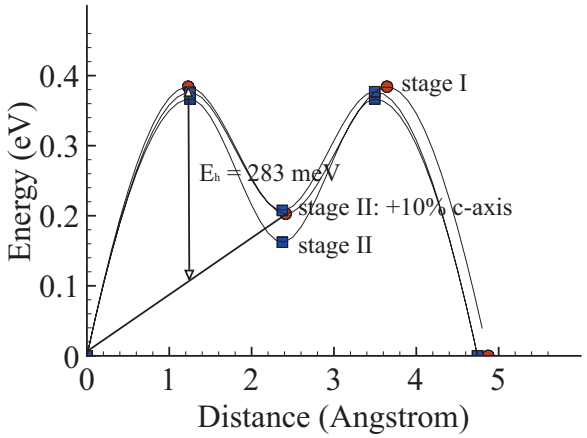

FIG. 10. (Color) Energy barriers calculated from first principles in stage II (blue squares) and stage I (red circles), in the high Li content limit. The result clearly shows that the energy barrier in the high Li concentration limit is the same for both stage I, and stage II as well as independent of increased interlayer distance.

TABLE II. First-principles activation barriers, calculated with the nudged elastic band method, for stage I and stage II compounds in dilute/nondilute limits. The Li concentrations are given as in-plane concentrations where the fully lithiated plane would correspond to LiC_6.

Compound class	In-plane Li concentration x (Li_xC_6)	E_h (meV)
Stage II	1/3	218
Stage II	2/3	283
Stage I	2/3	293

dilute Li concentrations, where the nearest in-plane Li-Li distance is 7 A (well outside the range of the Li-Li in-plane pair interaction as deduced from the cluster expansion) and nondilute in-plane Li concentrations which is calculated as the completely filled layer with Li vacancies at least 7 A apart (corresponding to an in-plane Li concentration of approximately 0.7). In the dilute limit [see Fig. 8(a)], the hopping Li are unaffected by other Li and only one migration barrier is relevant. We investigated whether the Li migration barrier is influenced by the number of (a least one) empty layers between the layer in which Li hops. By calculating the Li migration barrier in stage II (one empty layer between each Li hopping layer) as well as stage IV (3 empty layers between each Li hopping layer), we found that the barrier is the same for dilute stage II as for dilute stage IV [see Fig. 8(b)]. This is in agreement with our results from the CE, which find very little Li-Li interaction extending beyond one empty graphene-graphene layer. Moreover, we find that the dilute stage II migration barrier is very low (218 meV) for the equilibrium stage II cell parameters but *very dependent* on the grapheme-graphene interlayer distance, see Fig. 8(b). For example, we note that decreasing the interlayer spacing by 10% doubles the Li migration barrier, which would significantly impact the in-plane Li diffusion in the system.

We can distinguish between two local hop environments for nondilute Li concentrations: the "vacancy" hop [Fig. 9(a)] and the NN hop [Fig. 9(b)], where the name indicates the end point site for the hopping Li. The NN hop passes through a C-C bridge very close to another Li (2.17 Å) while the vacancy hop crosses the C-C bridges at a distance of 3.3 Å from the closest neighboring Li. These differences in in-plane Li-Li interactions lead to significantly different migration barriers for the two hop environments. At equilibrium lattice conditions for stage I, the NN hop has a migration barrier of ~1 eV, while the vacancy hop occurs at 283 meV. For stage II, the vacancy hop is 297 meV, which is only 15 meV higher than for stage I and within the error margin of elastic band calculations. Increasing or decreasing the interplane distance did not significantly affect the activation barriers (in either stage I or stage II)—see Fig. 10—for either hop, indicating that the limiting factor for diffusion at high Li concentrations comes from local in-plane Li-Li interactions. Comparing to the first-principles LDA calculations of Li migration barriers in ordered LiC_6 in Ref. 22, we find that our Li migration barrier is approximately 100 meV lower, for the equivalent Li-vacancy hop. This is likely a direct result of the overbinding of LDA in the treatment of the Li-graphite system[24] which affects phase stability as well as Li migration barriers.

Given the sensitivity of the migration barrier to the graphene-graphene spacing in the dilute Li concentration limit and our difficulty in reproducing the interlayer distance at low Li content with GGA, we chose to perform the kinetic Monte Carlo simulations in the nondilute case only. For the kinetic Monte Carlo we use a direction-independent barrier

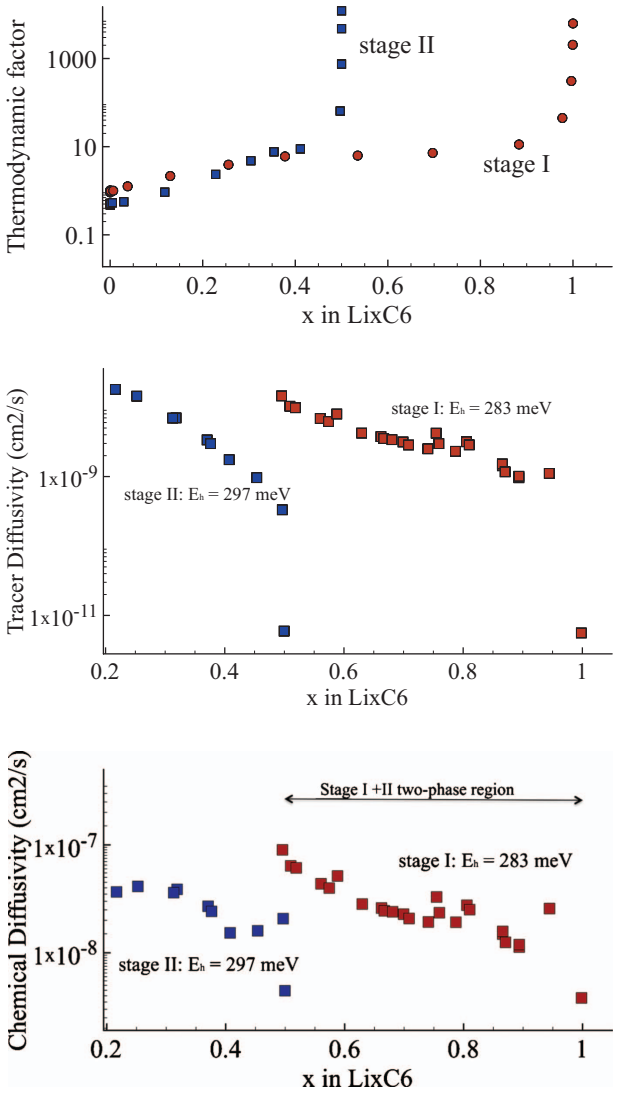

FIG. 11. (Color) (a) Thermodynamic factor for stage I (red circles) and stage II (blue squares) compounds, calculated with Monte Carlo simulations. (b) The self-diffusivity for stage I (red circles) and stage II (blue squares) calculated with kinetic Monte Carlo simulations. Both stage I and stage II are calculated using the barriers for the high Li concentration limit (E_h=283 meV for stage I and E_h=297 meV for stage II). (c) The chemical diffusivity for stage I (red circles) and stage II (blue squares) obtained from the tracer diffusivity and the thermodynamic factor. Both stage I and stage II are calculated using the barrier for the high Li concentration limit (E_h=283 meV in stage I and E_h=297 meV in stage II). We emphasize that the pure ordered phases are only observed at their stoichiometric compositions and that the stable phase for $0.5<x<1$ is the two-phase mixture.

model,[49] where the average of the energies of the end points of the hop are subtracted from the energy at the activated states. The kinetically resolved activation barriers used in the kinetic Monte Carlo runs for the nondilute stage I and stage II cases are given in Table II. The nondilute stage II results are given for $x>0.3$ which corresponds to 2/3 of the Li layer sites filled and constitutes a reasonable limit for where the Li layer concentration can be considered nondilute. The thermodynamic factor, shown in Fig. 11(a), was calculated with grand canonical Monte Carlo simulations. Figures 11(b) and 11(c) show the tracer diffusivity and chemical diffusivity I for stage II and stage I phases for the relevant concentration ranges. At 300 K, Li ions in stage II order at $x=0.5$ while in stage I they order at $x=1.0$. Li ordering leads to sharp dips in the tracer diffusivity and peaks in the thermodynamic factor. The chemical diffusivity, which is obtained by multiplying the tracer diffusivity with the thermodynamic factor [Eq. (2)], shows some fluctuations around the ordering composition and a distinct drop at the exact ordering. As can be seen in Fig. 11(c), the chemical diffusivity in stage II for $0.3<x<0.5$ is almost identical to the diffusivity in stage I for $0<x<1$, if the concentration scale is adjusted to account for *in-layer* concentration, rather than overall concentration ($x_{\text{stage I}} \rightarrow 2x_{\text{stage II}}$). This implies that the Li diffusivity is primarily determined by the in-plane Li concentration and interactions, and that empty layers between highly populated layers do not greatly impact in-layer diffusivity.

We find that, as a function of increasing Li concentration, the chemical diffusivity in graphite slowly decreases. This is a direct result of repulsive in-plane Li-Li interactions, which inhibit Li mobility at higher Li content. Apart from the ordering effects, i.e., some fluctuations and a sharp decrease in diffusivity at $x=0.5$ and $x=1.0$, there are no other significant features in the diffusivity trend with concentration. It is difficult to compare the absolute diffusivity with experimental data, which spans $10^{-7}-10^{-14}$ cm^2/s (see Refs. 15–17). One explanation for this inconsistency between different experimental results may be that the techniques used are based on planar models using a geometric area to calculate the Li diffusivity, which is very different with the actual electrochemical interface area.[16] Another explanation may reside in the directional dependence of Li diffusion in graphite particles. Li intraplanar diffusion, accessed by the graphene edge surfaces, is evidently much faster than defect-induced *interlayer* diffusion through the basal planes.[53] The present calculations pertain to bulk intraplanar graphite diffusion, without any surface effects or bulk defects. Thus, we can conclude that the Li graphite system has inherently very high bulk diffusivity and that actual rate limitations in this system likely originate from crystallinity, surface, particle morphology effects, and/or the solid-electrolyte interface formation.

IV. CONCLUSIONS

The current work presents results from first-principles calculations and statistical mechanics simulations of the thermodynamics and kinetics of Li_xC_6. We find that this system can be well studied in the high Li concentration limit ($x>0.5$ in Li_xC_6), using density-functional-theory methods together with a simple correction for the vdW binding energy between the graphene planes. Our cluster expansion shows that Li-Li interactions, in the Li-graphite system, are well-represented by repulsive short-range pair interactions. By correcting for vdW interactions between the graphene planes it is possible to reproduce the experimentally observed sequence of phases as a function of Li content. Thus, the staging of phases observed in the Li-graphite system is a direct consequence of the competition between Li-Li repulsive interactions and C-C attractive vdW interactions. While the Li-Li interactions would prefer a homogenous Li concentration in all planes, so as to minimize the Li-Li distances, the vdW interaction benefits from keeping some planes free of Li. By combining the cluster-expansion methodology to describe the energy of Li order/disorder in stage II and stage I compounds with Monte Carlo simulations we were able to predict the Li_xC_6 phase diagram in good agreement with experiment for high Li concentrations ($x>0.5$).

We also investigated Li diffusion in Li_xC_6 as a function of Li concentration. We find that at dilute Li concentrations, the Li migration barrier is very dependent on the interlayer slab space while at high Li content the limiting factor for diffusion is in-plane Li-Li interactions as opposed to the slab space. We calculated Li-diffusion coefficients as a function of Li concentration for $x>0.2$ in Li_xC_6 using first-principles migration barriers together with cluster expansions for the Li-vacancy configurational energy in kinetic Monte Carlo simulations. We find that intraplanar Li diffusion in graphite follows a smooth, slowly decreasing curve as a function of Li concentration. Most importantly, our calculations show that inherent Li diffusivity in bulk graphite is very fast which implies that rate limitations in this system likely originate from surface and/or crystallinity effects.

ACKNOWLEDGMENTS

Work at the Lawrence Berkeley National Laboratory was supported by the Assistant Secretary for Energy Efficiency and Renewable Energy, Office of Vehicle Technologies of the U.S. Department of Energy, under Contract No. DE-AC02-05CH11231. Work at the Massachusetts Institute of Technology was supported by Ford Motor Co. under Grant No. 014502-010. Anton van der Ven acknowledges support from NSF under Grant No. DMR 0748516.

[1] W. A. van Schalkwijk and B. Scrosati, *Advances in Lithium-Ion Batteries* (Springer, New York, 2002).
[2] D. A. Stevens and J. R. Dahn, J. Electrochem. Soc. **148**, A803 (2001).
[3] J. R. Dahn, Phys. Rev. B **44**, 9170 (1991).
[4] K. C. Woo, W. A. Kamitakahara, D. P. DiVincenzo, D. S. Robinson, H. Mertwoy, J. W. Milliken, and J. E. Fischer, Phys. Rev. Lett. **50**, 182 (1983).
[5] K. Co. Woo, H. Mertwoy, J. E. Fischer, W. A. Kamitakahara, and D. S. Robinson, Phys. Rev. B **27**, 7831 (1983).
[6] D. P. Di Vincenzo, C. D. Fuerst, and J. E. Fischer, Phys. Rev. B **29**, 1115 (1984).
[7] D. P. DiVincenzo and T. C. Koch, Phys. Rev. B **30**, 7092 (1984).
[8] S. A. Safran and D. R. Hamann, Phys. Rev. B **22**, 606 (1980).
[9] J.-S. Filhol, C. Combelles, R. Yazami, and M.-L. Doublet, J. Phys. Chem. C **112**, 3982 (2008).
[10] M. Inaba, H. Yoshida, Z. Ogumi, T. Abe, Y. Mizutani, and M. J. Asano, J. Electrochem. Soc. **142**, 20 (1995).
[11] T. Ohzuku, Y. Iwakoshi, and K. Sawai, J. Electrochem. Soc. **140**, 2490 (1993).
[12] A. Hightower, C. C. Ahn, B. Fultz, and P. Rez, Appl. Phys. Lett. **77**, 238 (2000).
[13] S. A. Solin, Adv. Chem. Phys. **49**, 455 (1982).
[14] Y. Imai and A. Watanabe, J. Alloys Compd. **439**, 258 (2007).
[15] N. Takami, A. Satoh, M. Hara, and I. Ohsaki, J. Electrochem. Soc. **142**, 371 (1995).
[16] H. Yang, H. J. Bang, and J. Prakash, J. Electrochem. Soc. **151**, A1247 (2004).
[17] P. Yu, B. N. Popov, J. A. Ritter, and R. E. White, J. Electrochem. Soc. **146**, 8 (1999).
[18] D. Morgan, A. Van der Ven, and G. Ceder, Electrochem. Solid-State Lett. **7**, A30 (2004).
[19] B. Kang and G. Ceder, Nature (London) **458**, 190 (2009).
[20] M. W. Verbrugge and B. J. Koch, J. Electrochem. Soc. **150**, A374 (2003).
[21] K. Toyoura, Y. Koyoma, A. Kuwabara, and I. Tanaka, J. Phys. Chem. C **114**, 2375 (2010).
[22] K. Toyoura, Y. Koyama, A. Kuwabara, F. Oba, and I. Tanaka, Phys. Rev. B **78**, 214303 (2008).
[23] N. A. W. Holzwarth, S. G. Louie, and S. Rabii, Phys. Rev. B **30**, 2219 (1984).
[24] K. R. Kganyago and P. E. Ngoepe, Phys. Rev. B **68**, 205111 (2003).
[25] C. Hartwigsen, W. Witschel, and E. Spohr, Phys. Rev. B **55**, 4953 (1997).
[26] W. Lehnert, W. Schmickler, and A. Bannerjee, Chem. Phys. **163**, 331 (1992).
[27] J. Kohanoff, G. Galli, and M. Parrinello, J. Phys. IV **01**, C5-351 (1991).
[28] H. Rydberg, M. Dion, N. Jacobson, E. Schroder, P. Hyldgaard, S. I. Simak, D. C. Langreth, and B. I. Lundqvist, Phys. Rev. Lett. **91**, 126402 (2003).
[29] J. P. Perdew, K. Burke, and M. Ernzerhof, Phys. Rev. Lett. **77**, 3865 (1996).
[30] G. Kresse and J. Furthmuller, Comput. Mater. Sci. **6**, 15 (1996).
[31] H. Rydberg, N. Jacobson, P. Hyldgaard, S. I. Simak, B. I. Lundqvist, and D. C. Langreth, *Hard Numbers on Soft Matter* (Elsevier Science Bv, New York, 2003), pp. 606–610.
[32] P. E. Blöchl, Phys. Rev. B **50**, 17953 (1994).
[33] G. Kresse and D. Joubert, Phys. Rev. B **59**, 1758 (1999).
[34] J. M. Sanchez, F. Ducastelle, and D. Gratias, Physica A **128**A, 334 (1984).
[35] D. de Fontaine, *In Solid State Physics; Advances in Research and Applications*, edited by H. Ehrenreich and D. Turnbull, (Academic Press, New York, 1994), Vols. 33 and 47.
[36] M. Asta, C. Wolverton, D. de Fontaine, and H. Dreysse, Phys. Rev. B **44**, 4907 (1991).
[37] G. Ceder, A. Van der Ven, C. Marianetti, and D. Morgan, Modell. Simul. Mater. Sci. Eng. **8**, 311 (2000).
[38] V. Ozoliņš, B. Sadigh, and M. Asta, J. Phys.: Condens. Matter **17**, 2197 (2005).
[39] M. Asta, V. Ozolins, and C. Woodward, JOM **53**, 16 (2001).
[40] A. Van der Ven, M. K. Aydinol, G. Ceder, G. Kresse, and J. Hafner, Phys. Rev. B **58**, 2975 (1998).
[41] C. Wolverton and A. Zunger, Phys. Rev. Lett. **81**, 606 (1998).
[42] M. E. Arroyo y de Dompablo, A. Van der Ven, and G. Ceder, Phys. Rev. B **66**, 064112 (2002).
[43] A. Van der Ven and G. Ceder, Electrochem. Commun. **6**, 1045 (2004).
[44] Y. Hinuma, Y. S. Meng, K. Kang, and G. Ceder, Chem. Mater. **19**, 1790 (2007).
[45] Y. Hinuma, Y. S. Meng, and G. Ceder, Phys. Rev. B **77**, 224111 (2008).
[46] A. Van der Ven, J. C. Thomas, Q. Xu, B. Swoboda, and D. Morgan, Phys. Rev. B **78**, 104306 (2008).
[47] A. van de Walle and G. Ceder, J. Phase Equilib. **23**, 348 (2002).
[48] G. Mills, H. Jonsson, and G. K. Schenter, Surf. Sci. **324**, 305 (1995).
[49] A. Van der Ven, G. Ceder, M. Asta, and P. D. Tepesch, Phys. Rev. B **64**, 184307 (2001).
[50] L. Benedict, N. G. Chopra, M. L. Cohen, A. Zettl, S. G. Louie, and V. H. Crespi, Chem. Phys. Lett. **286**, 490 (1998).
[51] M. K. Aydinol, A. F. Kohan, and G. Ceder, *Ab Initio Calculation of the Intercalation Voltage of Lithium Transition Metal Oxide Electrodes for Rechargeable Batteries* (Elsevier Science Sa, New York, 1997), pp. 664–668.
[52] V. Meunier, J. Kephart, C. Roland, and J. Bernholc, Phys. Rev. Lett. **88**, 075506 (2002).
[53] K. Persson, V. A. Sethuraman, L. J. Hardwick, Y. Hinuma, Y. S. Meng, A. van der Ven, V. Srinivasan, R. Kostecki, and G. Ceder, J. Phys. Chem. Lett. **1**, 1176 (2010).